Computational evaluation of experimental methodologies of out-of-plane behaviour of framed-walls with openings

Filip Anić,[1] Davorin Penava,[1] Lars Abrahamczyk,[2] and Vasilis Sarhosis[3]

[1] Faculty of Civil Engineering Osijek, Josip Juraj Strossmayer University of Osijek, Osijek 31000, Croatia.
[2] Earthquake Damage Analysis Center (EDAC), Bauhaus-Universität Weimar, Weimar D-99421, Germany.
[3] School of Engineering, Newcastle University, Newcastle upon Tyne, NE4 5TG, United Kingdom.

Correspondence should be addressed to Davorin Penava; davorin.penava@gfos.hr

Abstract

Framed masonry wall structures represent a typical high rise structural system and thusly, a seismically vulnerable one. During the ground motions, they are excited in both in-plane and out-of-plane manner. The interaction between the frame and the infill is a highly investigated phenomena in the field of seismic engineering. This paper presents a numerical investigation of two different static out-of-plane loading methods on framed masonry wall models. The first, most common method is uniformly loaded infill. The load is generally induced by the airbag. The other method is similar to in-plane push-over method, that is, loading the frame directly, not the infill. Consequently, openings with the same area but different size compositions and placements were examined. The numerical model is based on calibrated in-plane bare frame model and also on calibrated wall models subjected to OoP bending. Both methods produced widely divergent results in terms of load bearing capabilities, failure modes, damage states and etc. Summarily, uniform load on the panel causes more damage to the infill than to the frame; openings do influence structures behaviour; three hinged arching action is developed; and greater resistance and deformations are obtained in comparison to the frame loading method. Loading the frame causes the infill to bear significantly greater damage than the infill; infill and openings influence the behaviour only after reaching the peak load; infill does not influence initial stiffness; models with opening fail at same inter storey drift ratio as the bare frame model.

Introduction

Many cities are located on seismically active zones and usually they contain seismically vulnerable high rise buildings. High rise buildings are generally made either from reinforced concrete (RC) or structural steel frames that are infilled with some kind of masonry panels. During the earthquake, ground motion excites the structure and correspondingly, frames interact with the infill walls. This interaction is heavily investigated in the field of seismic engineering. The ground motion excites frames in some arbitrary direction, although, its affect can be generalized into three main components: a) In-plane (IP) behaviour; b) Out-of-plane (OoP) behaviour; c) Combination: previous IP damage on OoP behaviour (IP+OoP) and the opposite (OoP+IP). Majority of research was done in the field of IP behaviour, while less in the field of OoP behaviour, especially for their combination [1].

The OoP behaviour is thoroughly investigated by the field of seismic and blast engineering. The ingrained OoP experimental test are done by fixing the frame and loading the infill wall. Those walls are mostly uniformly loaded with airbags [2–6], and occasionally with point [7,8] or line loads [9]. This approach is certainly a great method for blast engineering, but also for wind and soil induced OoP load. During the ground motions, frames are excited as well, not fixed. This is well exhibited in real structures as in Figure 1. Nevertheless, due to inertial forces the infill is exited as well. As shown in dynamical studies by [10], panel and frame have different natural frequencies even thou they moved as a single unit. Tests where the loading was set on the frame rather than the infill were conducted by [11,12] as a previous OoP damage for IP analysis. The relation between the methods of loading the infill and loading the frame is largely unknown.

Loading in OoP direction, especially when loaded with airbags was found to produce beneficial arching action as found by [13]. By developing arching action, structures achieve greater load bearing and deformation capabilities. Various parameters can limit or even bypass the arching action, such as boundary conditions [4], openings [4,14–16], slenderness of the infill [17], frame stiffness [16], mortar and masonry characteristics [2,18] and other. Due to arching action, the largest displacements occur near the panels mid-height.

Canadian provisions [19] and those of New Zealand limit calculating OoP capacities via arching action theories (do not specify the equation). Others such as US Masonry joint committee [20] prescribe the use of Dawe and Seah's equation [16], while FEMA 356 [21] prescribes the use of modified Angels [22] equation. Both equations are based on the arching action theory. On the other hand, Eurocode 8 provisions [23] limit the slenderness of infill to $h/t < 15$. If the slenderness is greater than 15, additional actions of strengthening should be arranged.

Consequently, this paper considers a numerical investigation on OoP behaviour of one-storey, one-bay RC frame with unreinforced masonry infill (URM) wall loaded with both uniform load on the infill and point loads on the frame. RC frames with URM infill is a common practice in seismically active South Europe [24]. The study was conducted using Atena3D software [25]. Frames and URM's geometrical and material properties are obtained from [26,27]. The aim is to compare the two approaches and observe the influence of openings.

This paper also considers various types of openings, as their influence on OoP behaviour is yet to be investigated systematically. The present studies with openings show opposing results. On one hand, in the studies by [4,16], openings did not result in lowering the ultimate force. However, the deformation capabilities were significantly lowered. On the other hand, in the studies by [14,15] the reduction of ultimate force and deformation was observed for both window and door opening. This was also observed in URM wall experiments as in [28] and RC walls test in [29]. Mays [29] also provides formula for linear reduction of ultimate force based on the size of the opening, however, his observation was based on RC walls not framed masonry.

| a) Final stage of a specimen from in-situ tests with URM walls | b) A confined masonry building during Chi-Chi Earthquake, 1999 |

Figure 1 OoP failures in framed masonry structures (Figures obtained from [30])

General information

Structure, with a scale of 1:2.5 from Figure 2 was used to assemble the numerical model. RC frames can be classified by EN 1992-1-1 [31] & EN 1998-1-1 [23] provisions as medium ductility class frames (DCM). Hollow clay masonry blocks used as infill units are classified as Group II by the EN 1996-1-1 [32] provisions. General purpose mortar was used and is classified as M5 by EN 1996-1-1 [32] provision.
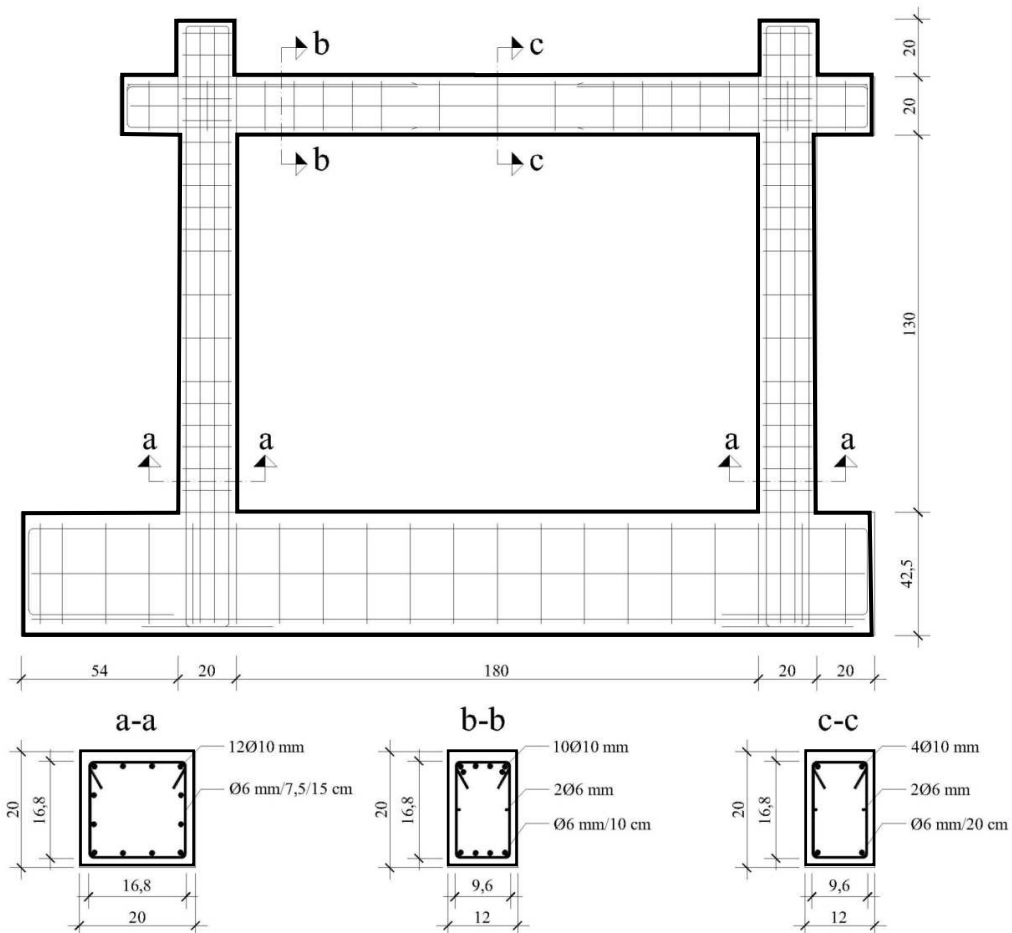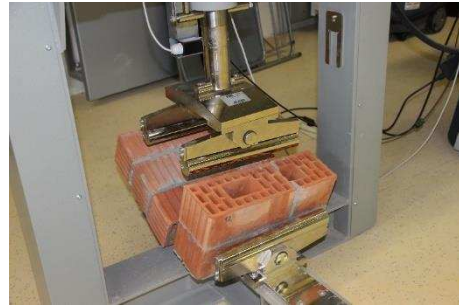

Figure 2 Reinforcement plan [33]
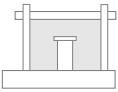
| a) Load parallel to headjoints | b) Load parallel to bedjoints |
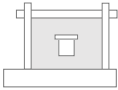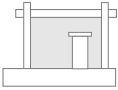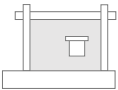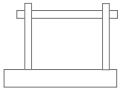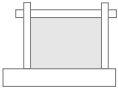
Figure 3 Wall specimens tested on OoP bending

Table 1 lays out specimens used for the numerical analysis. Originally, they were tested for cyclic-quasi static IP tests by [33]. The opening area (A_o) was selected to be 2.0 m^2 which falls within the range (i.e., $A_o > 1.5$ m^2 and $A_o > 2.5$ m^2) defined by EN 1998-1 [23]. Hence, the opening size does not vary, but its position and proportions do.

Table 1 Specimens considered

Model Mark	Appearance of the specimen	Opening	
		Type and area	Position
CD		Door $l_o / h_o = 0.35 / 0.90$ m $A_o = 0.32$ m^2 $A_o / A_i = 0.14$	Centric $e_o = l_i / 2 = 0.90$ m
CW		Window $l_o / h_o = 50.0 / 60.0$ cm $A_o = 0.30$ m^2 $A_o / A_i = 0.13$	Centric $e_o = l_i / 2 = 0.90$ m $P = 0.40$ m
ED		Door $l_o / h_o = 0.35 / 0.90$ m $A_o = 0.32$ m^2 $A_o / A_i = 0.14$	Eccentric $e_o = h_i / 5 + l_o / 2 = 0.44$ m
EW		Window $l_o / h_o = 50.0 / 60.0$ cm $A_o = 0.30$ m^2 $A_o / A_i = 0.13$	Eccentric $e_o = h_i / 5 + l_o / 2 = 0.44$ m $P = 0.40$ m
BF		Bare frame	
FI		Full infill	

4

In order to investigate differences and similarities between two approaches, the problem was separated into:

Approach 1: OoP load is transmitted onto the infill with uniform load (airbag method);

Approach 2: OoP load is transmitted onto the frame (inter storey drift method).

Boundary conditions for the Approach 1 were assembled in a way to mimic the conditions such as in [16,34,35]. In those studies, the beam was fixed from translation and airbag transmitted uniform area load on the infill. In the case of openings, as in [4], plywood was used to cover the opening. In the studies present in this paper, the opening was not covered and loaded. For the Approach 2, the conditions are mimicking [36] testing. In the study, two forces were applied on each column. One actuator was placed at the beam-column joint, and other one at columns mid-height. In studies presented in this paper, only the force at beam-column joint was placed.

Materials and Methods

Materials

The mechanical properties of the infill are presented in Table 2 and properties of RC in Table 3. Due to presence of voids in the block, material orthogonality is pronounced and stronger response is obtained in direction of voids then perpendicularly.

Length
25.0 cm

Width
12.0 cm

Height
9.5 cm
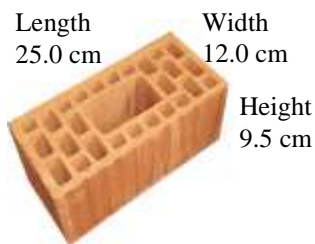
Figure 4 Clay masonry block used as infill units

Figure 5 Interlock effect in real structure [33]

Additional OoP bending test were carried out in accordance with EN 1052-2 [37] provisions. Tests were initiated in order to obtain the infill's OoP behaviour characteristics. Results are presented in [27], in short, it was found that when the line of the load is parallel with the bedjoints, wall fails by separating blocks, i.e. reaching tension strength of the mortar. When the line load is perpendicular to bedjoints, wall fails by cracking trough the block.

Table 2 Masonry properties obtained by tests

Specimen	Properties	Value	Unit
Clay block [33]	f_b	15.90	MPa
	f_{bh}	2.60	MPa
Mortar [33]	f_m	5.15	MPa
	f_{mt}	1.27	MPa
Wall specimen [33]	f_k	2.70	MPa
	E	3900.00	MPa
	ε_u	0.58	‰
	f_{vk0}	0.35	MPa
	$\mathrm{tg}\alpha_k$	0.24	MPa
Wall specimens OoP bending [27]	f_x	0.21	MPa
	f_{xh}	0.36	MPa

Table 3 RC properties obtained by tests (obtained from [33])

Entity	Properties		Value	Unit
Concrete	Compressive strength	f_c	58	MPa
	Yield stress	f_y	550	MPa
Rebar	Tension strength	f_t	650	MPa
	Elasticity modulus	E	197430	MPa

CC Nonlinear Cementitious material model [38] was used to describe behaviour of clay block and concrete. The input values are shown in Table 4. It is to be noted that all values, except of tensile strength for the case of clay block in Table 4 represent values tested in the direction of voids. The tensile strength perpendicular to the voids was introduced in order to have reliable OoP bending simulation [27].

Interface material model [38], meaning the contact between solid elements is presented in Table 6. Interlocking effect (Figure 5) occurs as mortar is laid on the blocks, mortar slips into the voids and therefore locks two opposite blocks in simulations action. Interlocking effect was introduced to the interface material model by the interlocking functions (Figure 6).

Table 4 CC Nonlinear Cementitious 2 material model

Description	Symbol	Frame concrete	Concrete lintel	Clay block	Unit
Elastic modulus	E	4.100E+04	3.032E+04	5.650E+03	MPa
Poisson's ratio	μ	0.200	0.200	0.100	/
Tensile strength	f_t	4.000	2.317	0.380	MPa
Compressive strength	f_c	-5.800E+01	-2.550E+01	-1.750E+01	MPa
Specific fracture energy (eq.3)	G_f	1.200E-04	5.739E-05	4.500E-04	MN/m
Crack spacing	s_{max}	0.125	0.125	/	m
Tensile stiffening	c_{ts}	0.400	0.400	/	/
Critical compressive disp.	W_d	-5.000E-04	-5.000E-04	-5.000E-04	/
Plastic strain at f_c	ε_{cp}	-1.417E-03	-8.411E-04	-1.358E-03	/
Reduction of f_c due to cracks	$r_{c.lim}$	0.800	0.800	0.800	/
Crack shear stiffness factor	S_F	2.000E+01	2.000E+01	2.000E+01	/
Aggregate size		1.600E-02	2.000E-02	/	m
Fixed crack model coefficient		1.000	1.000	1.000	/

Table 5 Bilinear steel reinforcement material properties

Description	Symbol	Value	Unit
Elastic modulus	E	2.10E+05	MPa
Yield strength	σ_y	5.50E+02	MPa
Tensile strength	σ_t	6.50E+02	MPa
Limited ductility of steel	ε_{lim}	0.01	/

Table 6 Interface material properties

Symbol	Mortar bedjoint Value	Mortar headjoint Value	Unit
K_{nn} (eq.1)	5.65E+05	8.50E+04	MPa
K_{tt} (eq.2)	2.57E+05	3.86E+04	MPa
f_t	0.20	0.20	MPa
c	0.35	0.35	MPa
tgα	0.24	0.24	/
Interlocking	see fig.6	/	

a) Interlocking function   b) Tension softening

Figure 6 Interface functions [39]
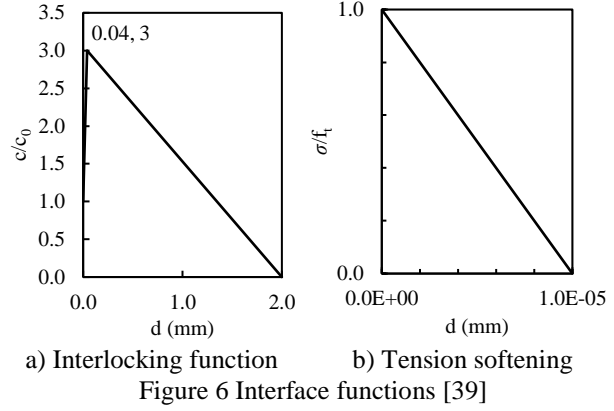
In the case of reinforcements, bilinear steel material model [38] was used, its values are shown in Table 5. Perfect connection between rebar and concrete was used.

$$K_{nn} = E / t \tag{1}$$
$$K_{tt} = G / t \tag{2}$$

Where t is mortar thickness (standard thickness of 10 mm).

$$G_f = 0.000025 \, f_t \tag{3}$$

As the frame represents a part of a bigger structure, compression force of 365 kN was introduced into the column ends. Such normal force produces noticeable friction forces T_F, and could not be undermined as it was shown on IP simulations of the same model [40]. Friction coefficient for sliding steel rollers, similar to ones used in the IP test (μ_F) was taken as 0.03 [41]. Hence, the friction force for one column end was calculated using Equation 4.

$$T_F = \mu_F \cdot 365 \approx 10 \, \text{kN} \tag{4}$$

For introducing friction force onto the numerical model, a non-linear surface spring was set on the columns. Spring stiffness calculated by Equation 5.

$$K_s = T_F / A_{col} = 0.25 \, \text{MPa} \tag{5}$$

The friction – spring function is presented in Figure 7. As the normal force is introduced, friction occurs immediately, hence small relative displacement was introduced before reaching full stress. A small incline was presented, ranging from 0.250 to 0.253 MPa in order to have greater numerical stability.

Figure 7 Nonlinear spring
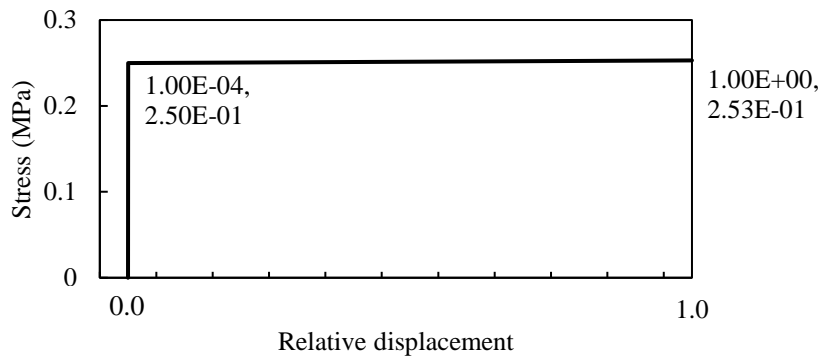
Numerical model setup

Numerical model of the frame (BF model) is based on the calibrated IP cyclic, quasi static model. Hence, the BF can be considered calibrated in OoP direction as well. The OoP characteristics of the infill were calibrated on bending tests (Fig. 3). The micromodel managed to mimic the failures and ultimate forces as in experiments. For further reads, please remark the reference [27].

Numerical models have the same setup up to the point of loading and supports. The characteristics that are identical for both Approaches are shown in Figure 8. Reinforcement was modelled as 1D truss bars. Rebar overlapping, was modelled by cumulating rebar areas and applying it to a single bar. Contacts between blocks and those between blocks and frame are modelled as gapped zero thickness (2D) interfaces, and other with perfect contact. The contact between the frame and infill do not contain interlocking functions as the interlocking effect cannot be developed on those areas. Brick mesh with size of 4 cm was applied to all elements. Few plate elements have triangulated surfaces mesh due to their geometrical irregularity.

a) Reinforcement 1D bar

b) Solid 3D macro elements

c) Contacts – 2D interface

d) FE mesh
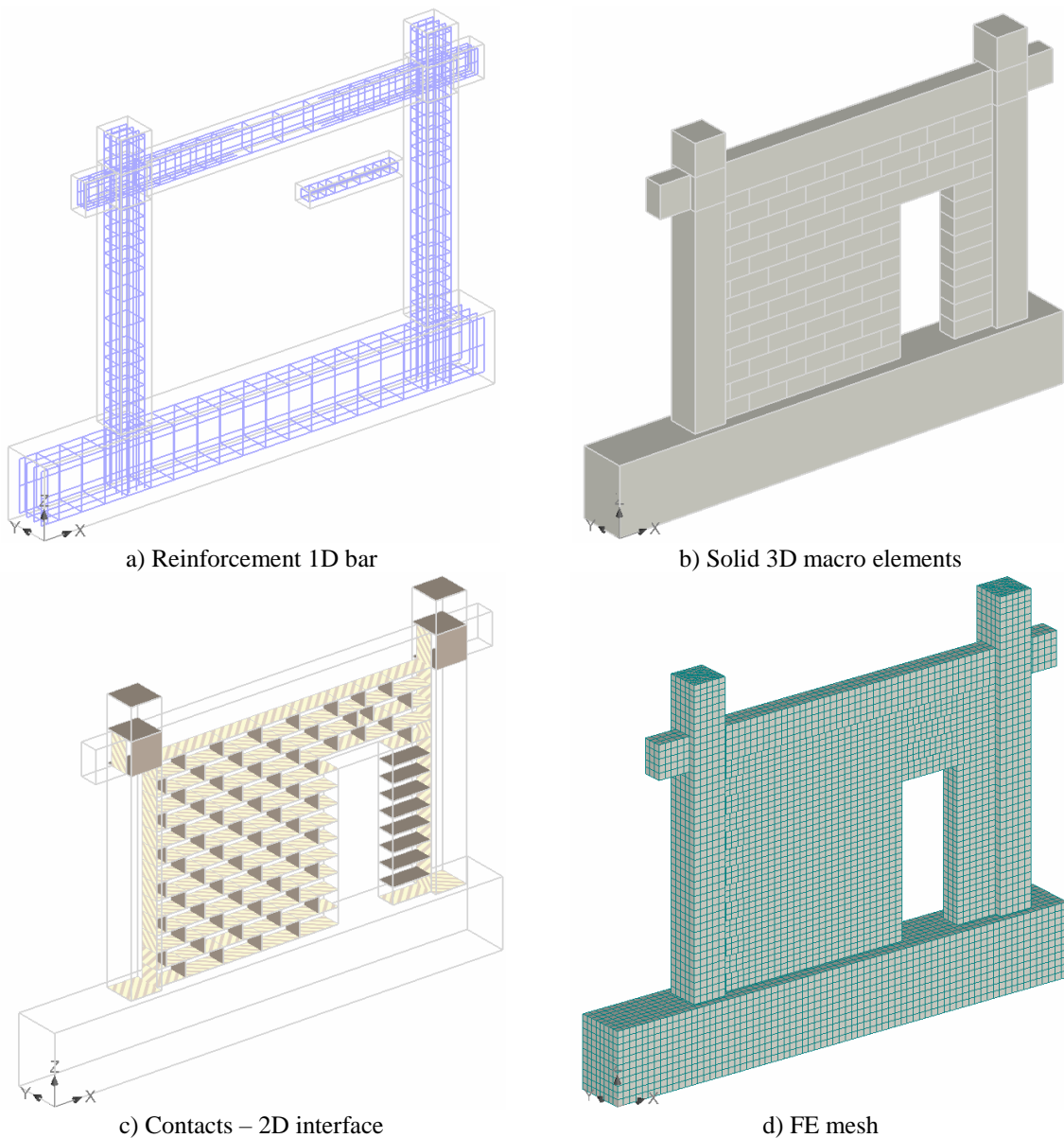
Figure 8 General model setup on ED model example

a) Supports for Approach 1   b) Supports for Approach 2

NL Spring

365 kN   365 kN

365 kN   365 kN

w

δ   δ

c) Loading for Approach 1   d) Loading for Approach 2
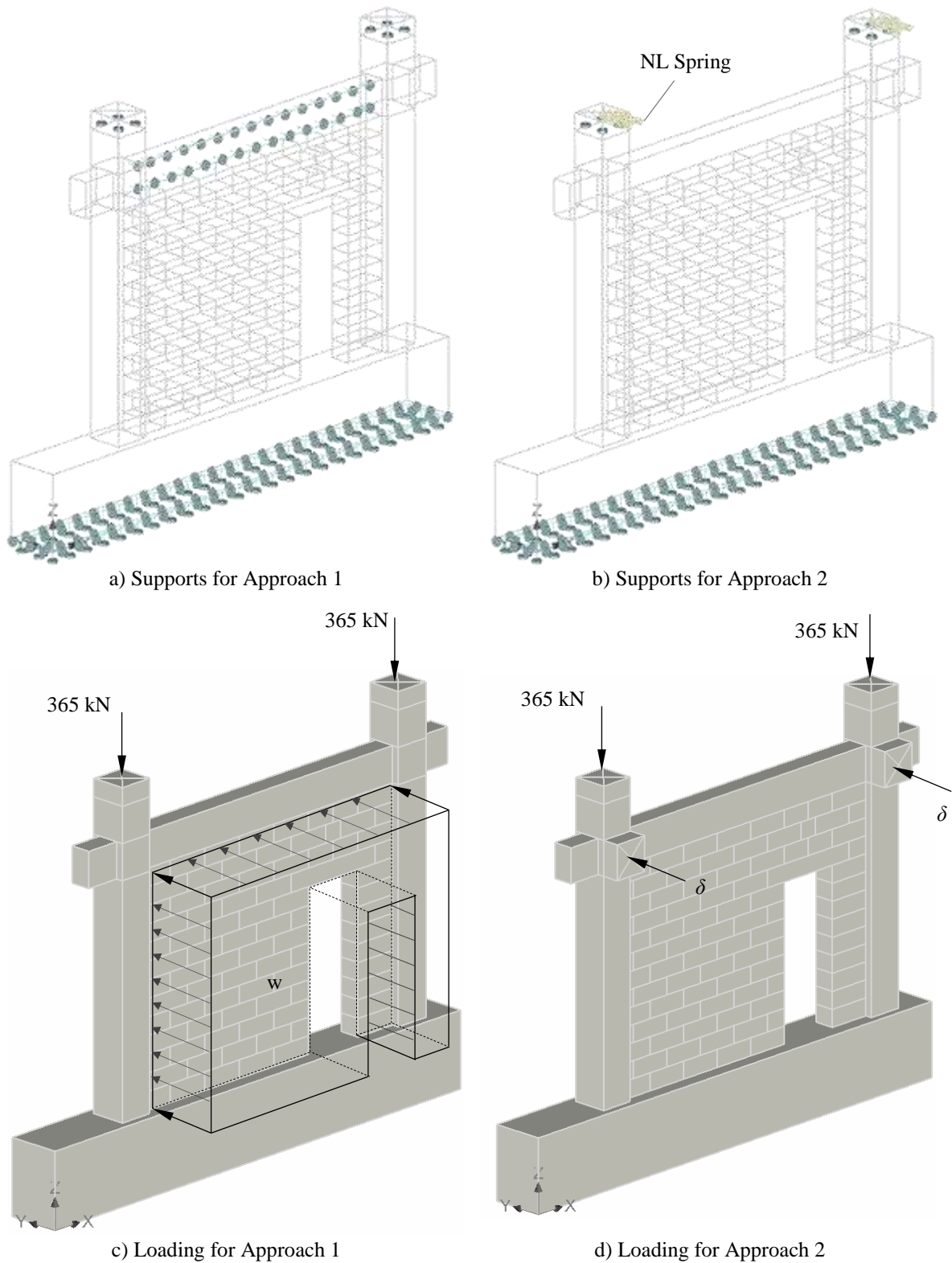
Figure 9 Boundary conditions on ED model example

On Figure **Error! Reference source not found.**, boundary conditions are shown. From there, it can be seen that both approaches have foundation supports fixed in all direction. Also, both approaches contain the vertical force of 365 kN, applied in 5 step with 73 kN increment. In the case of Approach 1 column support in z direction and beam supports in y direction are active as soon as the column force is applied. When the column support is activated, area load is set

9

on the infill with w = 0.002 MPa per step. On the other hand, in the case of Approach 2, after the vertical force is loaded, only column supports in z direction are active together with the non-linear spring in y direction to mimic the friction of the rollers. When the column supports are active, prescribed deformation is activated with deflection of δ = 0.1 mm per step. The model was pushed until it reached 2.5% drift ratio (d_r).

Results

In Figure 11, loading versus displacement diagram is shown with displacements and loadings plotted on primary horizontal and vertical axis. On the secondary vertical axis, load differences (Δw & ΔW) are presented. The referenced value, i.e. Δw & ΔW = 1 was set for the maximal force of the FI model. On the secondary horizontal axis, inter-storey drift ratios are plotted (d_r). For the Approach 1 (Fig.11a - d), displacement were measure as global maxima of the panel in y direction. Figures 11a,b & e are plotted to 2.5 % d_r, and Figures 11c & d, drift ratio was widen to 4% d_r in order to observe the yielding line. In the case of Approach 2, (Fig.11c), displacements were measured at point of load input, i.e. column – beam joint. On Figure 11a, area pressure w is shown, and in Figure 11b force W calculated using Equation 6. The force W from Figure 11c represents the sum of forces from each column.

$$W = w \ A_{infill}/A_{opening} \qquad (6)$$

On Figures 14 - 18, back side refers to the side that has the load applied, thus, the front view is then vice versa.
On Figure 12, minimum principal stress are plotted on the cross section of models in Approach 1. The section plane was positioned at the infills midlength in the case of FI model and right beside the opening for the models with opening.
On Figure 13 cracks patterns are shown for the Approach 1. Similarly, on Figure 16, crack patterns for Approach 2 are displayed.
On Figure 15, minimal principal stress at maximum drift ratio of the Approach 1 are shown. Similarly, on Figure 17 minimal principal stresses of the frame are shown and on Figure 18 minimal principal stresses of the infill are shown. Both figures represent stress at ultimate force.
On Figure 10, displacement in the y direction are displayed on the example of the CD model.

Discussions and conclusions

From Figure 11b, it is clear that in Approach 1 openings in regards to their composition and placement do effect the OoP behaviour. This was also found in the work by [14,15]. On the other hand, from Figure 11c it is noticeable that with Approach 2, the influence of openings are negligible in terms of forces and displacements before the peak load. In studies by [4,12] openings did not influence initial stiffness nor the ultimate force. The differences are noticeable after reaching the peak load. In detail, after reaching the peak load, models with openings do not defer from each other, and they obtain slightly greater forces in comparison to BF and slightly lower loads when compared to FI model. Moreover, models with openings fail at the same drift ratio as the BF model. The FI model showed more prominent behaviour after reaching peak load, as it did not fail, and the model acquired better post peak load bearing behaviour. With the Approach 2, it is noticeable that the infill does not influence the initial stiffness of the frame for the, although it influences post peak stiffness (Fig. 11d). The infills

negligible influence on the initial stiffness on the frames can be observed on dynamical studies results conducted on bare and infilled frames by [30].

From Figure 10 it is noticeable that displacement in the model from the Approach 2 range from zero at foundation to maximum at columns end. Likewise, it was found in the OoP studies on the shaking table test by [30]. In [10], maximal accelerations were observed at top of the panel. Furthermore, displacements of the infill and the frame are identical. Hence, frame and infill behave as single element. The same was found in dynamical tests by [10], where, relative and absolute displacements between the frame and the infill were nearly zero.

Torsion of the beam can be observed in Figure 10. The combination of torsion and translation of the beam can cause infill to lose the upper row as it was observed in an infill of a three storey building excited in OoP direction by a shaking table [30]. The effects of beams torsion was as well observed and implemented in calculation of OoP capacity by [16].

By examining Figures 12 & 17 it is clear that compression arch has developed for both models with and without openings. The FI model on Figure 12a, displays three supports where infill clamps: at the panels mid height, and at the beams. Those three points form the three hinged arching action (Fig. 13a) that is common with two – and one – way arching action. In the case of openings, there is accumulation of stress in the lintel (Fig. 12b-e & 17b-e), hence an additional support is formed. Hence, one can assume that a four – hinged action (Fig. 13b) form with additional point at the lintel. This additional hinge along with reduced area of the panel may cause the reduction of deformation capabilities as observed by [4].

Regarding the stress distribution for the Approach 2 (Fig.18), the ingrained arching action is not obvious. Rather, the two - hinged arching action (Fig.13) occurred. Though, the arch does not form but a compression thrust does. The prominent position of the two hinged action is found near the columns, due to same displacements on relation column – infill. The two - hinged action was also observed in shaking table test by [30].

When comparing minimum principal stress between frame and infill, it is noticeable that in the case of Approach 1, frame and infill obtain stress within the same range (Fig. 15). This resulted in heavy damage of the infill and slight damage to the frame. However, in the case of Approach 2, stress differ as much as ten times between the frame and the infill (Fig. 17 & 18).

Considering Figures 14 & 16, one can observe that in one hand with the Approach 1, there is heavy damage to the infill and on the other hand with the Approach 2 the infill is only slightly damaged, however, the frame acquired heavy damage. Figure 14 show that cracks, with and without openings, form the letter "X" pattern. The "X" pattern is typical occurrence as a result of a two – way arching action. Crack patterns in the case of Approach 2 are accumulated on the frame, and on the lower back side of panel (Fig. 16). Similar crack patterns were found in the studies by [30] with the two – hinged arching action.

Both Approaches developed corner crushing of the infill and managed to damage the frame at clamping points (Fig. 15 & 18). Both approaches developed tension around the bedjoints on the back view. The tension in the Approach 1 accumulated around the panel's midheight (Fig.15), and in the case of Approach 2 on the lower part of the infill (Fig. 18).

In conclusion, the two approaches display highly contrasting results. Namely, the accumulation of stress and thusly the damage in the case of the Approach 1 is in the infill and for the

Approach 2 in the frame. Hence, two different failure mechanisms occurred. In the Approach 1, three and four hinged arching action was developed and failure occurs by the infill. On the other hand, in the Approach 2, two hinged arching action occurred. Nevertheless, the frame failed, not the infill. The ultimate force is significantly greater in the case of the Approach 1, presumably as a result of developing arching action and different boundary conditions. In the case of Approach 1, infill contribution to the frame is unknown as there cannot be a reference to the bare frame specimens. Further on, in Approach 2 the infill did not influence initial stiffness nor the frames response before reaching the ultimate force. The influence of infill can be observed only after reaching peak load. Where the FI model had better load bearing and deformation capacities then the BF model. Also, unlike the BF model, the FI model did not fail at 2.5% d_r. Openings in Approach 1 did influence the load bearing capacities, and the arching action was able to develop. Hence, it can be considered that they influence the OoP behaviour. Given the Approach 2, openings affect the behaviour after reaching peak load. There, openings do not defer from each other in terms of load bearing capacitates and are somewhat between the FI and BF model. However, they fail at the same drift ratio as the BF model. Both Approaches showed considerable correlation with studies of the same loading method. Additionally, Approach 2 showed additional correlations with dynamical studies on shaking table.

References

[1]   Asteris PG, Cavaleri L, Di Trapani F, Tsaris AK. Numerical modelling of out-of-plane response of infilled frames: State of the art and future challenges for the equivalent strut macromodels. Eng Struct 2017;132:110–22. doi:10.1016/j.engstruct.2016.10.012.

[2]   Abrams DP, Angel R, Uzarski J. Out-of-Plane Strength of Unreinforced Masonry Infill Panels. Earthq Spectra 1996;12:825–44. doi:10.1193/1.1585912.

[3]   Hallquist Å. Lateral loads on masonry walls 1970.

[4]   Akhoundi F, Vasconcelos G, Lourenco P, Silva L. Out-of-plane response of masonry infilled RC frames : Effect of workmanship and opening. In: Modena C, F. da P, Valluzzi MR, editors. 16th Int. Brick Block Mason. Conf., Padova, Italy: CRC Press/Balkema; 2016, p. 1147–54.

[5]   Di Domenico M, Ricci P, Verderame GM. Experimental Assessment of the Influence of Boundary Conditions on the Out-of-Plane Response of Unreinforced Masonry Infill Walls. J Earthq Eng 2018:1–39. doi:10.1080/13632469.2018.1453411.

[6]   Furtado A, Rodrigues H, Arêde A. Numerical Modeling of masonry infill walls participation inthe seismic behavior of RC buildings. OpenSeesDays Port., Porto, Portugal: University of Porto; 2014.

[7]   Preti M, Migliorati L, Giuriani E. Experimental testing of engineered masonry infill walls for post-earthquake structural damage control. 2014. doi:10.1007/s10518-014-9701-2.

[8]   Hak S, Morandi P, Magenes G. Out-of-plane Experimental Response of Strong Masonry Infills. 2nd Eur. Conf. Earthq. Eng. Seismol., Istanbul, Turska: 2014.

[9]   Petrus C, Stoian V, Mosoarca M, Anastasiadis A. Reinforced Concrete Frames with Masonry Infills. Out of Plane Experimental Investigation. Researchgate.net n.d.

[10]   Fowler JJ. Analysis of dynamic testing performed on structural clay tile infilled frames. 1994.

[11]   Henderson R, Jones W, Burdette E, Porter M. The effect of prior out-of-plane damage on the in-plane behavior of unreinforced masonry infilled frames. Fourth DOE Nat. Phenom. Hazards Mitig. Conf., 1993, p. 18.

[12]   Flanagan R, Bennett R. Bidirectional behavior of structural clay tile infilled frames. J Struct Eng 1999;125:236–44. doi:10.1061/(ASCE)0733-9445(1999)125:3(236).

[13]   Gabrielsen B, Wilton C. Shock tunnel tests of arched wall panels 1974.

[14]   Wang C. Experimental investigation on the out-of-plane behaviour of concrete masonry infilled frames. Dalhousie University, 2017.

[15]   Sepasdar R. Experimental investigation on the out-of-plane behaviour of concrete masonry infilled RC frames. Dalhousie University, 2017.

[16]   Dawe JL, Seah CK. Out-of-plane resistance of concrete masonry infilled panels. Can J Civ Eng 1989;16:854–64. doi:10.1139/l89-128.

[17]   Moghaddam H, Goudarzi N. Transverse resistance of masonry infills. ACI Struct J 2010;107:461–7.

[18]   Mohamad G, Fonseca FS, Vermeltfoort AT, Martens DRW, Lourenço PB. Strength, behavior, and

failure mode of hollow concrete masonry constructed with mortars of different strengths. Constr Build Mater 2017;134:489–96. doi:10.1016/j.conbuildmat.2016.12.112.

[19]   Canadian Standards Association. Masonry design and construction for buildings 1978.

[20]   Masonry Standards Joint Committee and others. Building code requirements for masonry structures. Am Concr Institute, Detroit, MI, ISBN 1999;1929081022.

[21]   American Society of Civil Engineers (ASCE). FEMA 356 Prestandard and Commentary for the Seismic Rehabilitation of Building. Rehabilitation 2000.

[22]   Angel R, Abrams DP, Shapiro D, Uzarski J, Webster M. Behavior of reinforced concrete frames with masonry infills. University of Illinois Engineering Experiment Station. College of Engineering. University of Illinois at Urbana-Champaign.; 1994.

[23]   CEN. Eurocode 8: Design of Structures for Earthquake Resistance - Part 1: General Rules, Seismic Actions and Rules for Buildings (EN 1998-1:2004). Brussels: European Committee for Standardization; 2004.

[24]   Booth E, Key D. Earthquake Design Practice for Buildings. London: Thomas Telford; 2006.

[25]   Cervenka Consulting. ATENA for Non-Linear Finite Element Analysis of Reinforced Concrete Structures 2015.

[26]   Sigmund V, Penava D. Influence of openings, with and without confinement, on cyclic response of infilled R-C frames - An experimental study. J Earthq Eng 2014;18. doi:10.1080/13632469.2013.817362.

[27]   Anić, Filip; Penava, Davorin; Varevac, Damir; Sarhosis V. Influence of Clay Block Masonry Properties on the Out-of-Plane Behaviour of Infilled RC Frames. Teh Vjesn 2018.

[28]   Griffith MC, Vaculik J, Lam NTK, Wilson J, Lumantarna E. Cyclic testing of unreinforced masonry walls in two-way bending. Earthq Eng Struct Dyn 2007;36:801–21. doi:10.1002/eqe.654.

[29]   Mays GC, Hetherington JG, Rose TA. Response to blast loading of concrete wall panels with openings. J Struct Eng 1999.

[30]   Tu Y-H, Liu P-M, Lin H-P. Out-of-Plane Seismic Behavior of Unreinforced Masonry In-filled Walls. New Horizons Better Pract 2007:1–10. doi:10.1061/40946(248)48.

[31]   CEN. Eurocode 2: Design of concrete structures - Part 1-1: General rules and rules for buildings (EN 1992-1-1:2004). Brussels: European Committee for Standardization; 2004.

[32]   CEN. Eurocode 6: Design of masonry structures - Part 1-1: General rules for reinforced and unreinforced masonry structures (EN 1996-1-1:2005). Brussels: European Committee for Standardization; 2005.

[33]   Penava D. Utjecaj otvora na seizmičko ponašanje armiranobetonskih okvirnih konstrukcija sa zidanim ispunom. 2012.

[34]   Akhoundi F, Vasconcelos G, Lourenço PB, Palha C, Martins A. Out-of-plane behaviour of masonry infill walls. 7th Int. Conf. sesmiology Earthq. Eng., 2015.

[35]   Furtado A, Rodrigues H, Arête A, Varum H. Experimental Characterization of the In-plane and Out-of-Plane Behaviour of Infill Masonry Walls. Procedia Eng 2015;114:862–9. doi:10.1016/j.proeng.2015.08.041.

[36]   Henderson RC, Porter ML, Jones WD, Burdette EG. Influence of prior out-of-plane damage on the in-plane behavior of masonry infilled frames. TMS J 2006;24:71–82.

[37]   British Standards Institution. Methods of test for masonry Part 2: Determination of flexural strength. Bs En 1052-2 2016.

[38]   Cervenka V, Jendele L, Cervenka J. ATENA Program Documentation Part 1 Theory. Prague: Cervenka Consulting Ltd.; 2012.

[39]   Penava D, Sigmund V, Kožar I. Validation of a simplified micromodel for analysis of infilled RC frames exposed to cyclic lateral loads. Bull Earthq Eng 2016;14:2779–804. doi:10.1007/s10518-016-9929-0.

[40]   Anić F, Penava D, Sarhosis V. Development of a three-dimensional computational model for the in-plane and out-of-plane analysis of masonry-infilled reinforced concrete frames. COMPDYN 2017 - Proc. 6th Int. Conf. Comput. Methods Struct. Dyn. Earthq. Eng., vol. 2, 2017.

[41]   Hirt M, Lebet J-P. Steel Bridges: Conceptual and Structural Design of Steel and Steel-Concrete Composite Bridges. CRC Press; 2013.

Annotation

Mechanical (tested) properties	
f_b	Clay blocks normalized compression strength in direction of voids
f_{bh}	Clay blocks normalized compression strength in direction perpendicular to voids
f_m	Mortars compressive strength
f_{mt}	Mortars flexural strength
f_k	Characteristic masonry wall compressive strength
E	Elastic modulus of wall specimen
ε_u	Ultimate wall strain
f_{vk0}	Initial shear strength
$tg\alpha_k$	Friction coefficient

Other	
ΔW	Difference in pressure force
d_r	Drift ratio
δ	Prescribed deformation
w	Uniform area load
W	Point load
A_{col}	Column cross section area

Numerical material properties	
E	Elastic Modulus
μ	Poisson's coefficient
f_t	Tensile strength
f_c	Compressive strength
G_f	Fracture Energy
W_d	Plastic displacement
ε_{cp}	Strain at f_c
$r_{c,lim}$	Maximal strength reduction under the large transverse strain
S_F	Shear factor coefficient that defines a relationship between normal and shear crack stiffness.
K_{nn}	Normal interface stiffness
K_{tt}	Tangential interface stiffness
c	Cohesion
$tg\alpha$	Friction coefficient
V_R	Shear force
d	Displacement

Supplemental

Figure 10 Displacements of CD model at max. drift ratio d_r

a) Pressure vs. displacement – Approach 1

b) Force vs. displacement – Approach 1

c) Pressure vs. displacement – Approach 1

d) Force vs. displacement – Approach 1

e) Force vs. displacement – Approach 2

Figure 11 Load vs. displacement

15

a) FI b) CD c) CW d) ED e) EW

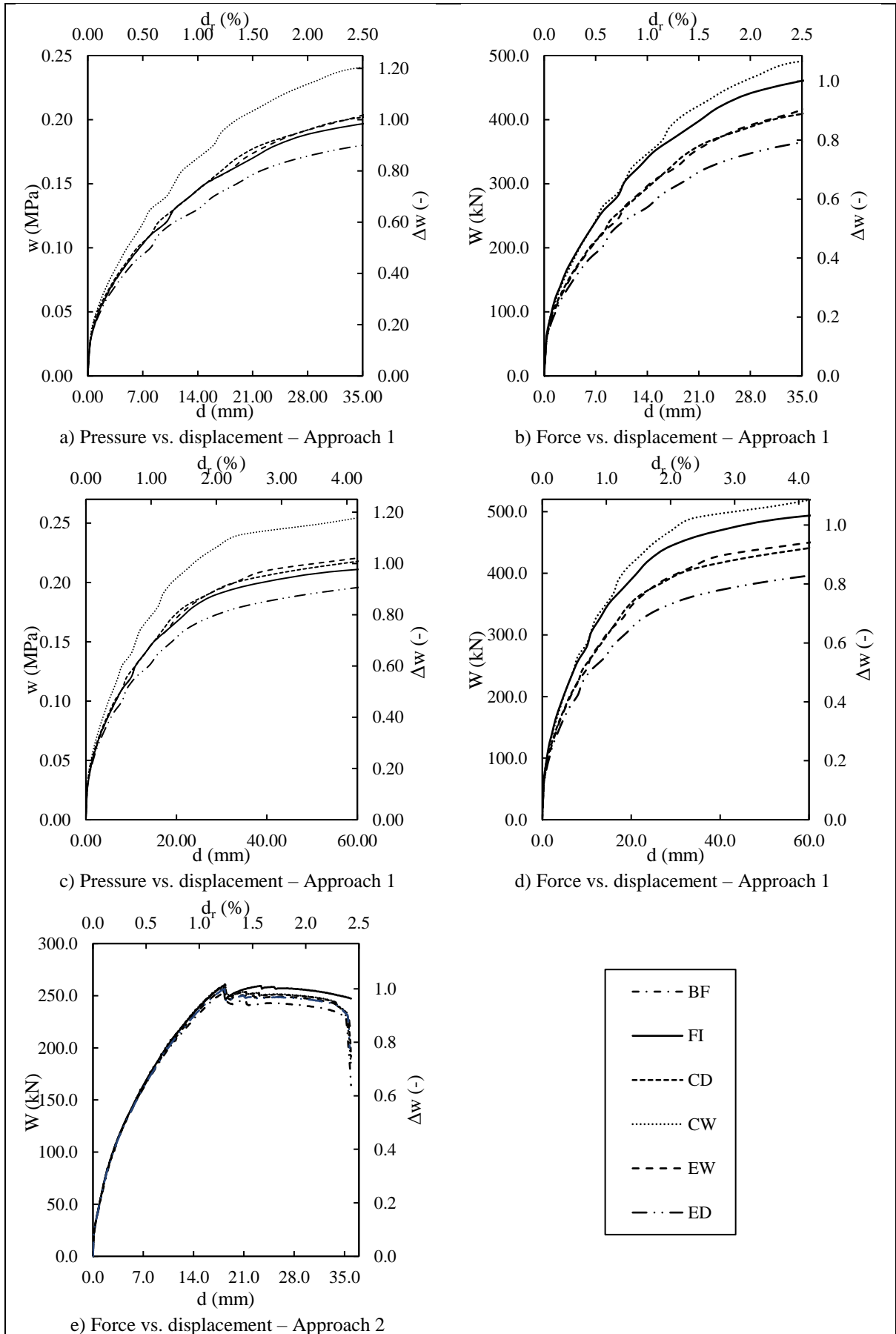σ_{min} (MPa)

0 -1 -3 -4 -5 -6 -8 -9 -10

< -10 > 0

Absolute deformation $\times 1$
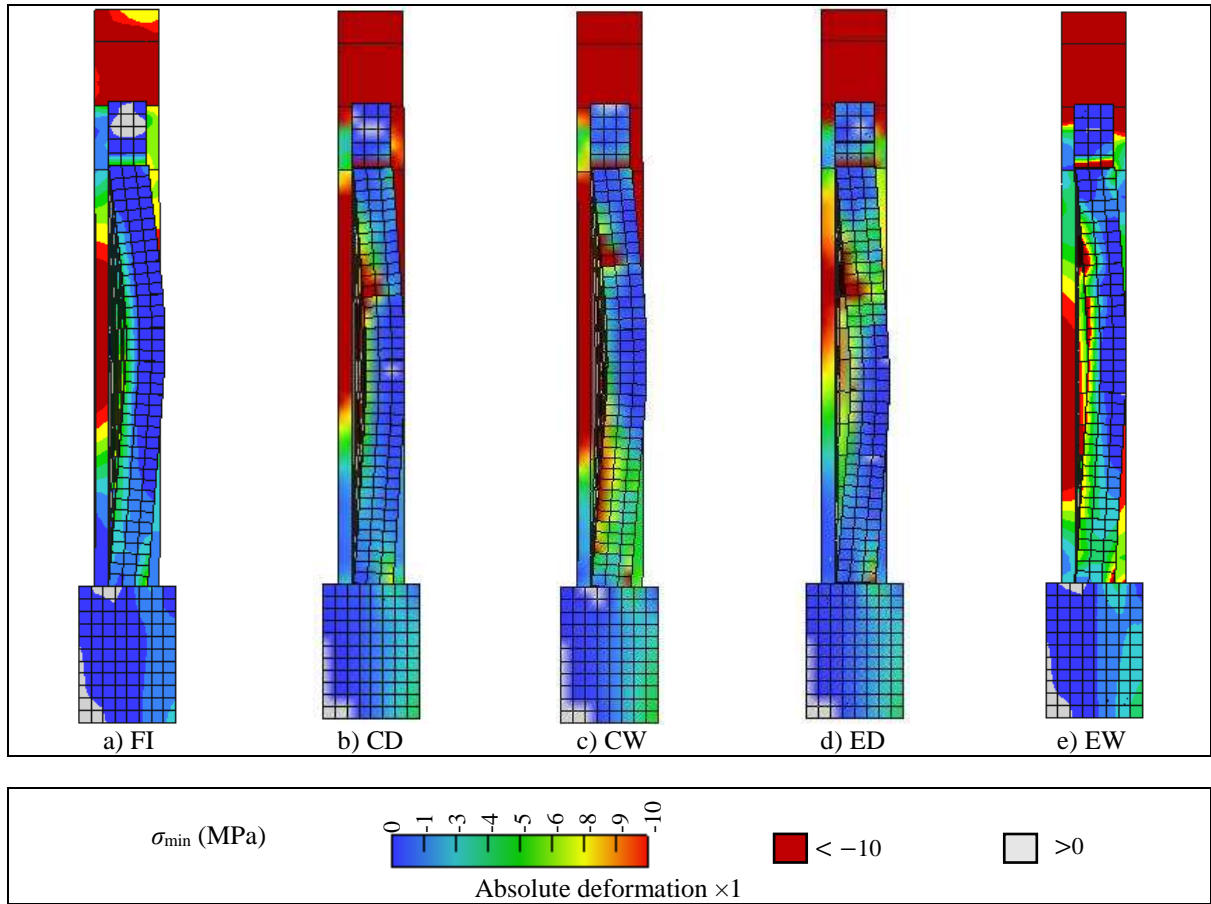
Figure 12. Approach 1: Minimum principal stress at max. displacement cross section

Lintel

a) Three hinged action   b) Four hinged action   c) Two hinged action
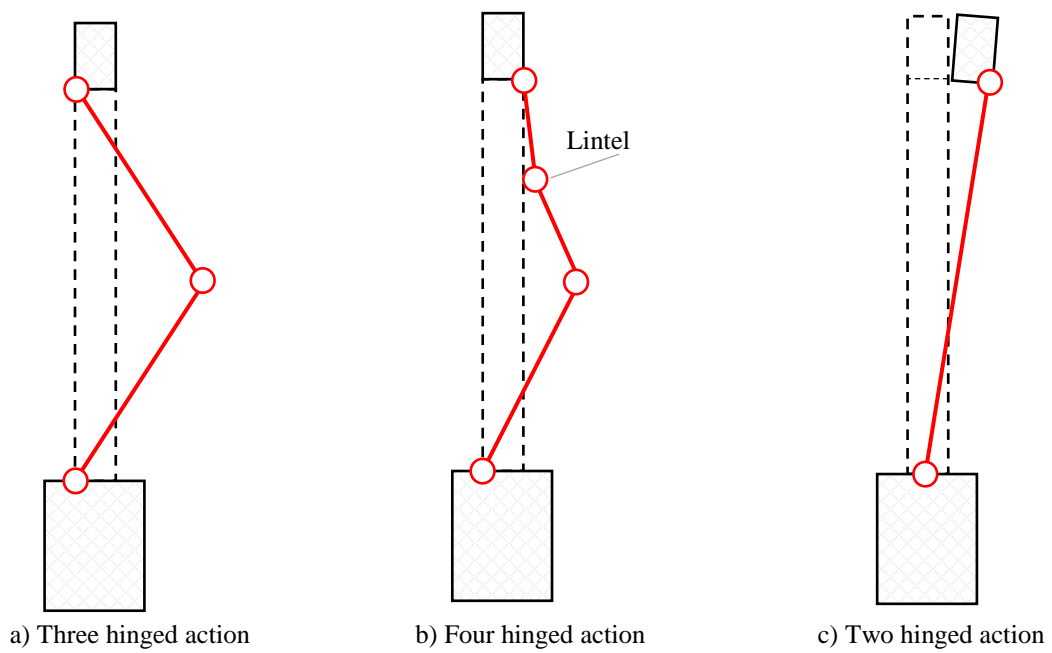
Figure 13 Arching actions as observed by Approach 1 & 2

a) FI model

b) CD model

c) EW model

d) ED model

e) EW model
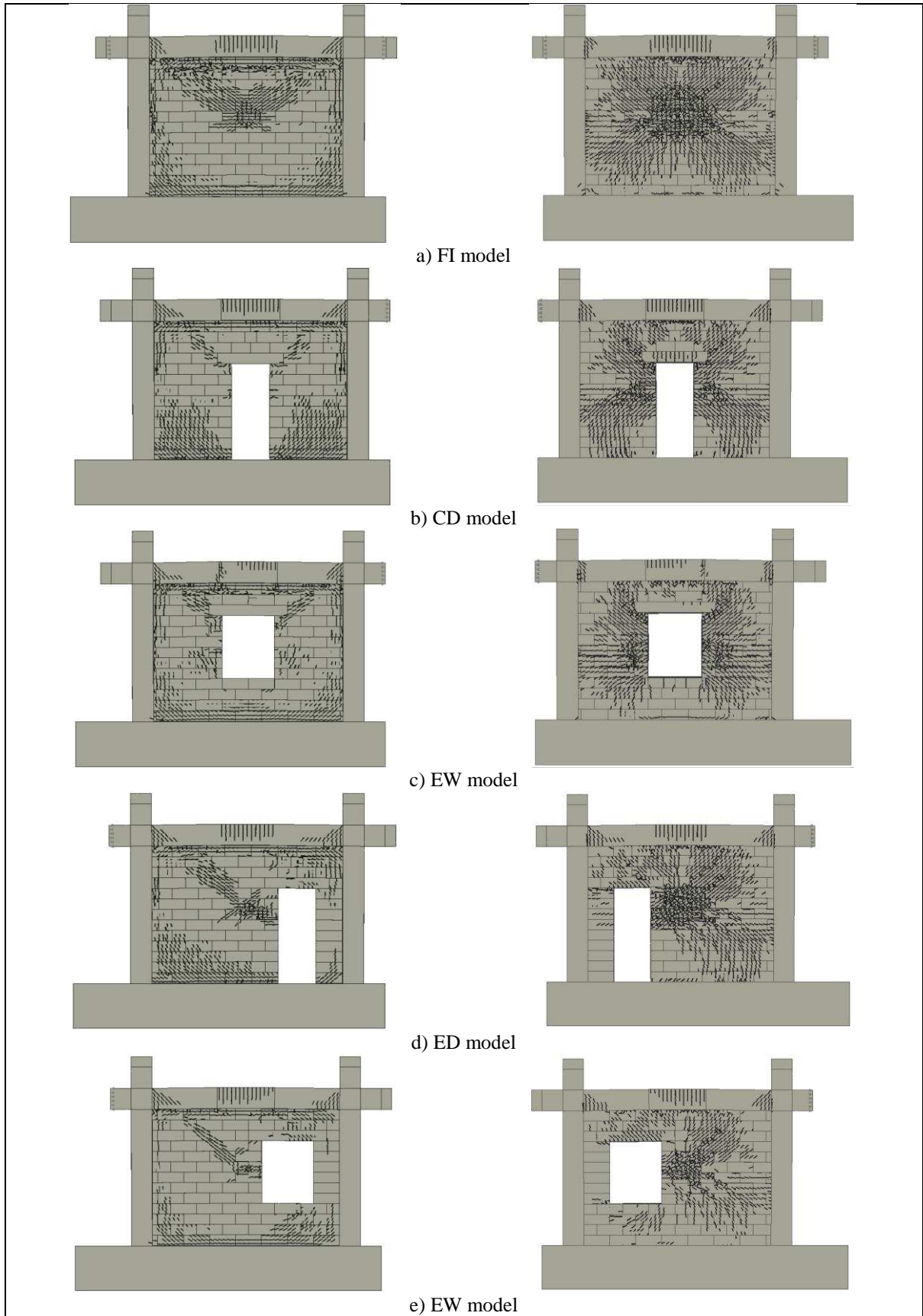
Min. crack width = 0.1 mm ; deformation × 1 ; crack width multiplier ×1

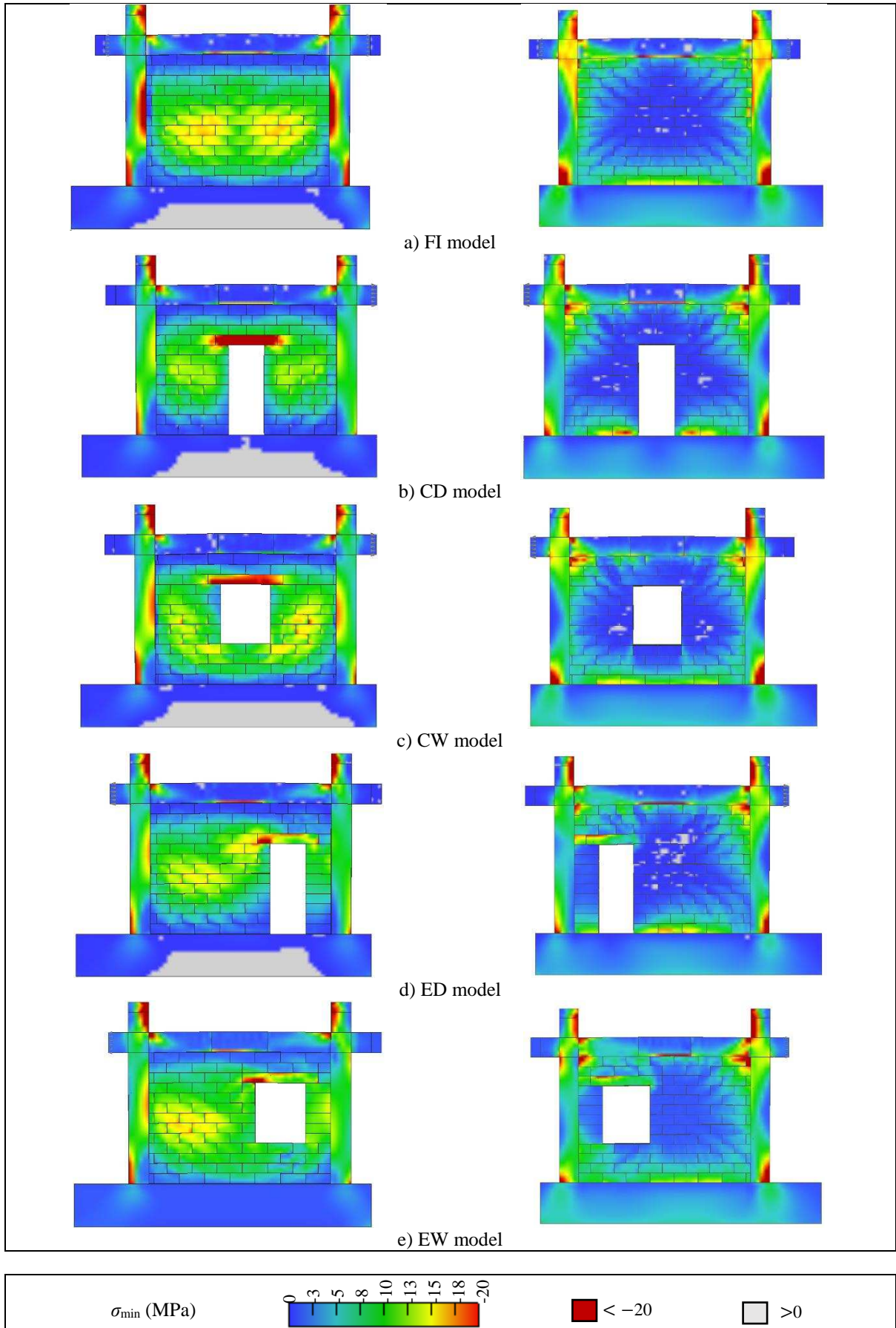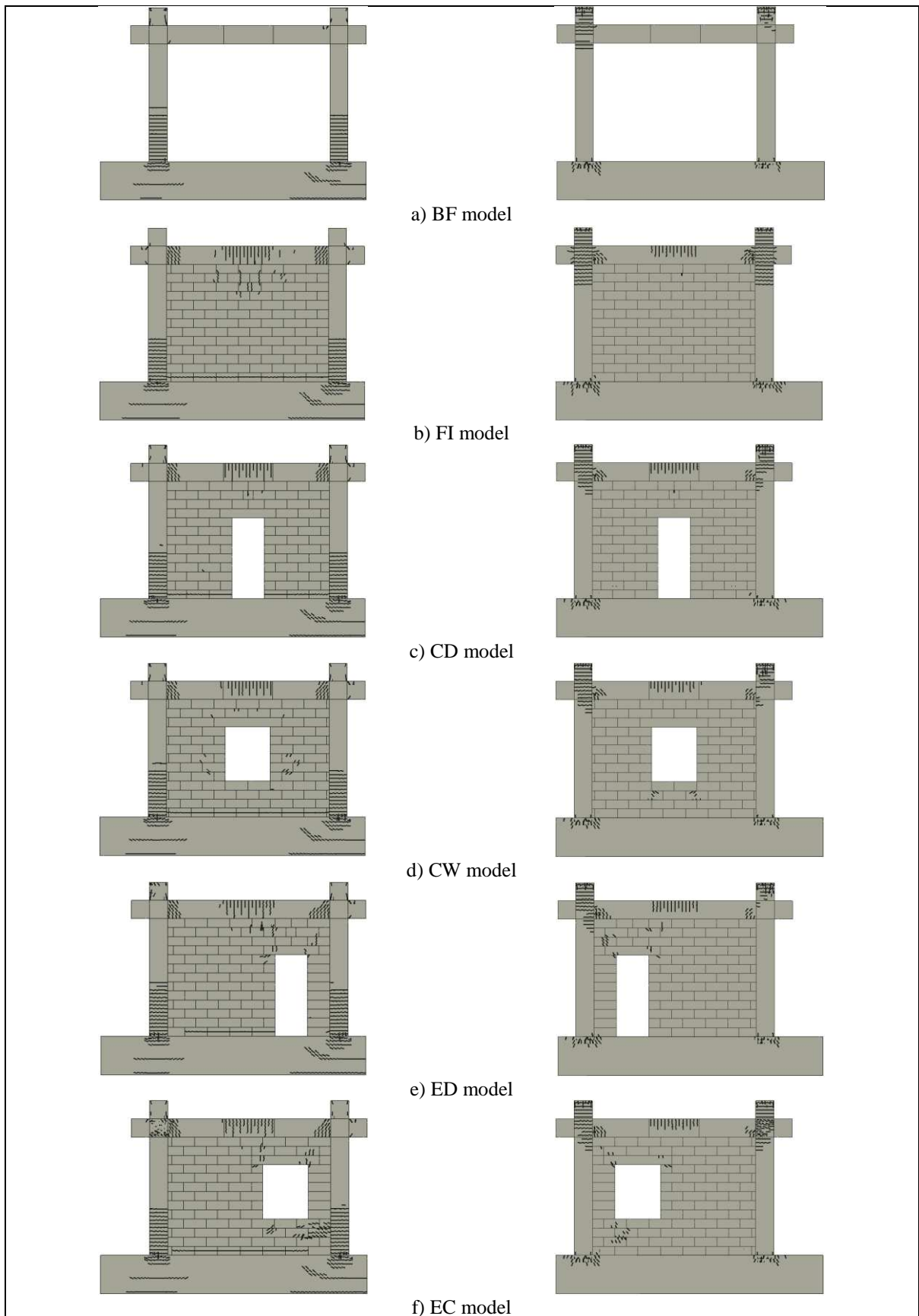Figure 14. Approach 1: Crack patterns (left front, right back view)

17

a) FI model

b) CD model

c) CW model

d) ED model

e) EW model

σ_{min} (MPa)   0 -3 -5 -8 -10 -13 -15 -18 -20 < -20 > 0

Figure 15. Approach 1: Minimum principal stress (left front, right back view)

a) BF model

b) FI model

c) CD model

d) CW model

e) ED model

f) EC model

Min crack width = 0.01 mm, Shift cracks outwards ×1, Crack width multiplier × 1, Deformation ×1

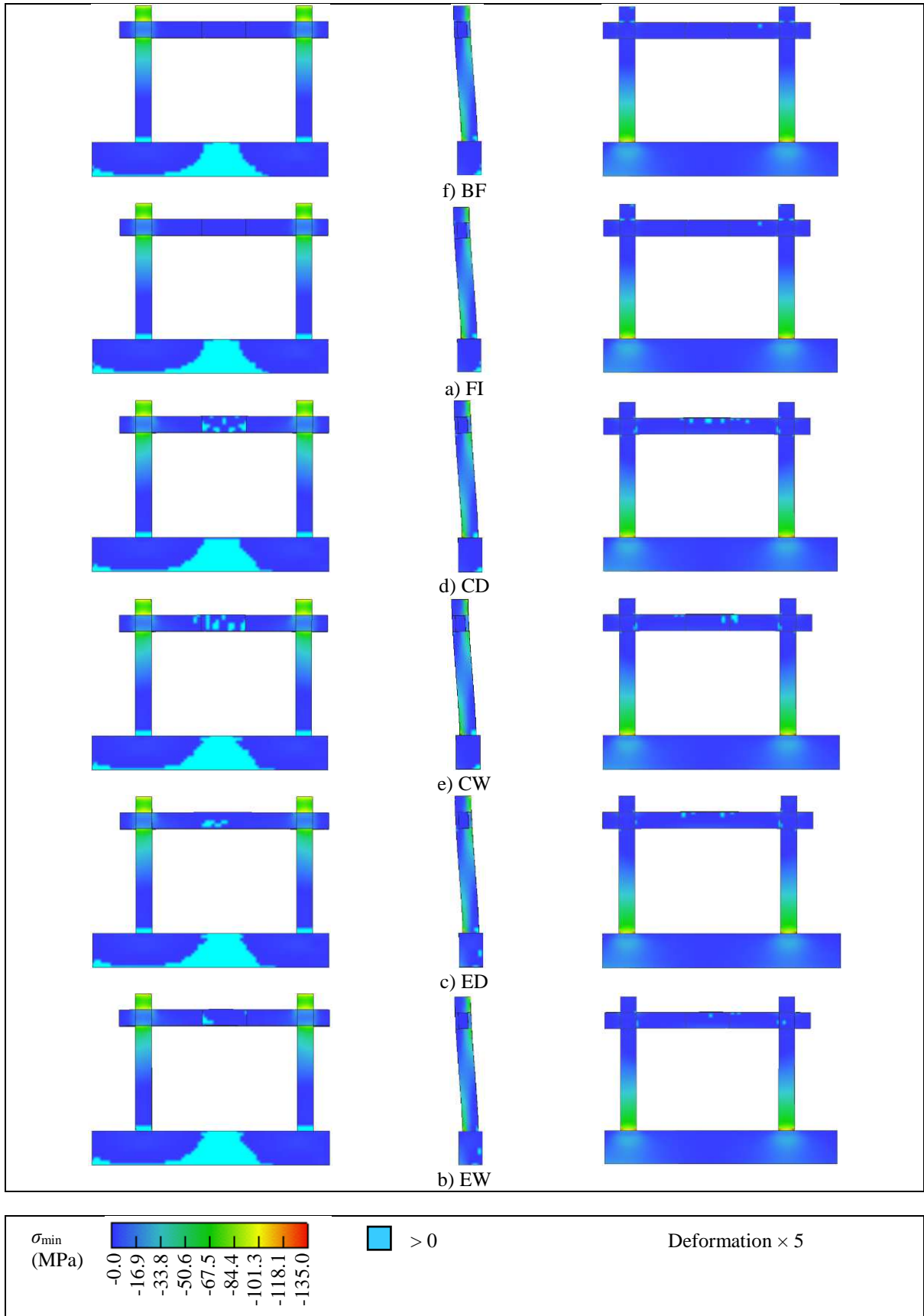Figure 16 Approach 2: Crack patterns maximum drift ratio d_r (left front, right back view)

f) BF

a) FI

d) CD

e) CW

c) ED

b) EW

σ_{min} (MPa) −0.0 −16.9 −33.8 −50.6 −67.5 −84.4 −101.3 −118.1 −135.0   > 0   Deformation × 5

Figure 17 Approach 2: Min. principal stress of the frame at max. force W (left front, right back view)

a) FI

b) CD

c) CW

d) ED

e) EW

σ_{min} (MPa)

-0.0 -1.38 -2.75 -4.13 -5.50 -6.88 -8.25 -9.63 -11.00
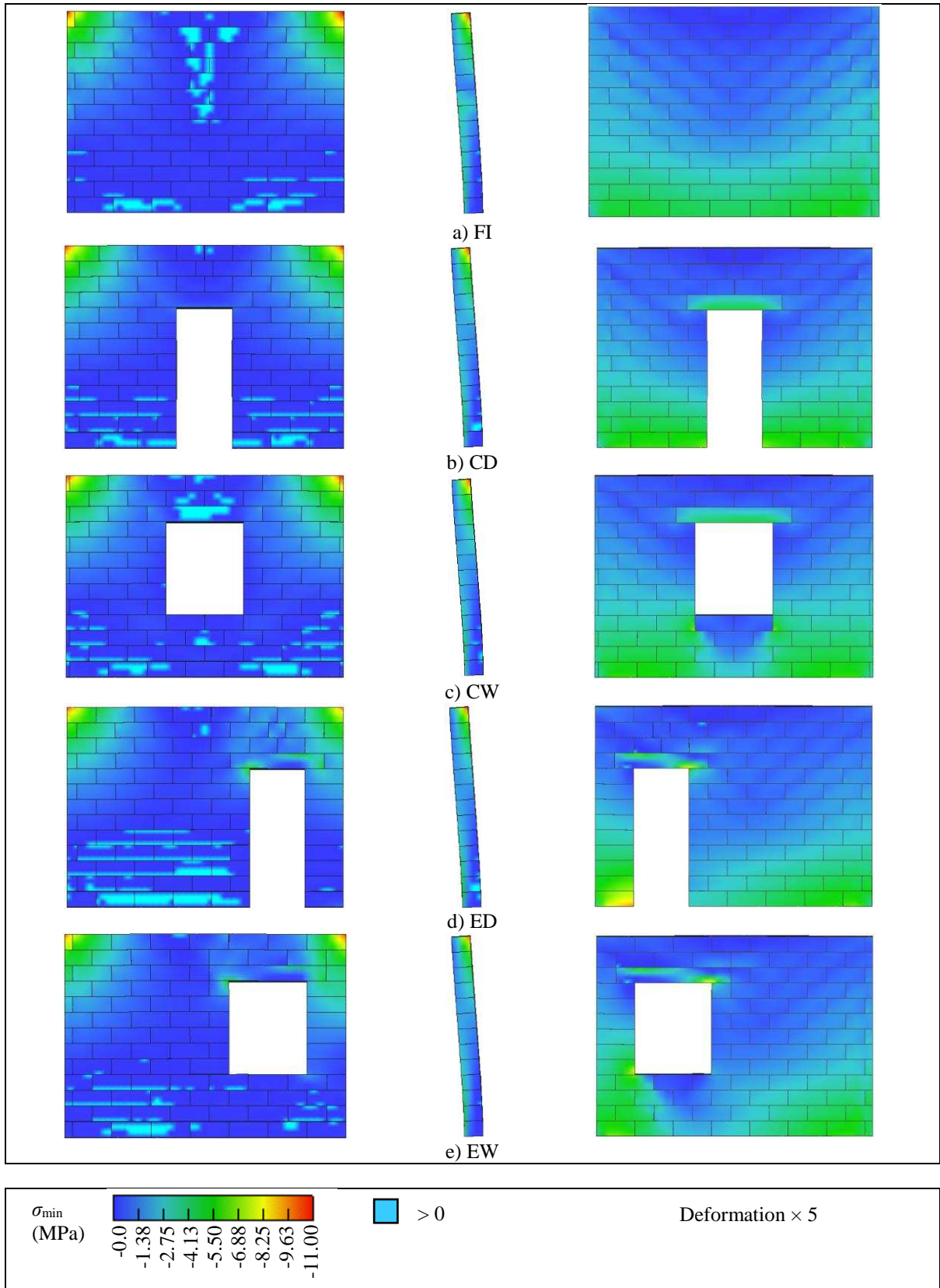
> 0

Deformation $\times$ 5

Figure 18 Approach 2: Min. principal stress in infill at max. force W (left front, right back view)